High-pressure falloff curves and specific rate constants for the reactions atomic hydrogen + molecular oxygen .dblharw. perhydroxyl .dblharw. hydroxyl + atomic oxygen

ARTICLE *in* THE JOURNAL OF PHYSICAL CHEMISTRY · JANUARY 1985

Impact Factor: 2.78 · DOI: 10.1021/j100248a033

3 AUTHORS, INCLUDING:

Carlos J. Cobos
National Scientific and Technical Research C…
126 PUBLICATIONS **3,038** CITATIONS

SEE PROFILE

of the 1,4-dimethylpyridinyl radical is one of the examples.[7]

Photochemical and Thermal Sequence. On the basis of the above results, the photochemical and thermal behaviors of the 1-methyl-4-*tert*-butylpyridinyl radical and the dimer can be illustrated with Scheme II.

Photochemical excitation of the dimer, followed by cleavage of the central C–C bond, leads to the formation of a singlet radical pair. The pairs undergo either recombination within the solvent cage or dissociation by escape from the cage. The latter forms isolated radicals which carry CIDEP observed in the time-resolved ESR spectra. The signal decays with the half-life of about 1 μs, the radicals finally going back to the dimer through the formation of a F pair. Concerning course of reaction, the escape of radicals from the solvent cage is understood from the small frequency factor for recombination, and the one-step decay of the ESR signal is indicative of direct formation of a 2,2 dimer, regardless of the large spin density at 4 position, because of the bulky *tert*-butyl group at that position.

Registry No. 1-Methyl-4-*tert*-butylpyridinyl radical, 93755-96-5; 1-methyl-4-*tert*-butylpyridinium iodide, 64326-91-6; 1,1′-dimethyl-4,4′-bipyridinium dichloride, 1910-42-5; 2,2′-bis(1-methyl-4-*tert*-butyl-2*H*-pyridine), 83864-59-9.

High-Pressure Falloff Curves and Specific Rate Constants for the Reactions $H + O_2 \rightleftharpoons HO_2 \rightleftharpoons HO + O$

C. J. Cobos,† H. Hippler, and J. Troe*

Institut für Physikalische Chemie der Universität Göttingen, D-3400 Göttingen, West Germany
(Received: June 27, 1984)

The recombination reaction $H + O_2 + M \rightarrow HO_2 + M$ is studied by laser flash photolysis in the bath gases M = Ar, N_2, and CH_4 at pressures between 1 and 200 bar. By extrapolation of the falloff curves, a limiting high-pressure rate coefficient $k_\infty = 7.5 \times 10^{-11}$ cm^3 molecule^{-1} s^{-1} is derived at 298 K. An analysis of this result in terms of the statistical adiabatic channel model leads to a looseness parameter of $\alpha \simeq 0.94$ Å^{-1}. The corresponding specific rate constants $k(E,J)$ for dissociation of HO_2 are constructed and compared with trajectory calculations. The results are also compared with data on the reaction $HO + O \rightarrow H + O_2$ for which a nearly temperature-independent rate constant of 2.8×10^{-11} cm^3 molecule^{-1} s^{-1} is predicted. An analysis of the limiting low-pressure rate coefficients with respect to energy-transfer properties is made. The results are compared with trajectory calculations of energy transfer of excited HO_2.

Introduction

The recombination reaction

$$H + O_2 + M \rightarrow HO_2 + M \quad (1)$$

plays an important role in many areas of chemical kinetics. It takes part in the HO_x cycle of atmospheric chemistry. As a chain quencher, it determines the second explosion limit of the hydrogen–(or hydrocarbon–) oxygen system; it also contributes to the heat release of many flames. In the gas phase, reaction 1 was investigated in numerous studies near to the low-pressure, third-order limit. Experiments have used the discharge-flow technique,[1-8] pulse radiolysis,[9-11] mercury photosensitization,[12-14] and the flash photolysis–resonance fluorescence technique.[15,16] There is evidence[17] that, besides HO_2 in the electronic ground state, also electronically excited HO_2 can be formed by reaction 1. In addition to the mentioned low-temperature studies, reaction 1 was investigated in shock waves and flames at high temperatures. A review of the available rate coefficients over wide temperature ranges has been given in several data compilations.[18-21] Surprisingly, so far nobody has tried to approach the high-pressure range of the reaction by using pressures above 1 bar. Our present work intends to close this gap by experimental studies in the range 1–200 bar.

Obtaining experimental information on the limiting high-pressure rate coefficient k_∞ of reaction 1 is of considerable theoretical and practical interest. An analysis of k_∞ in terms of unimolecular rate theory allows one to fix unknown parameters of the HO_2 potential energy surface or to test available potential energy calculations. This surface governs not only the kinetics of reaction 1, but also the important chain-branching process

$$H + O_2 \rightarrow HO + O \quad (2)$$

of many combustion systems and its reverse reaction

$$O + OH \rightarrow O_2 + H \quad (3)$$

With these reactions are connected the corresponding oxygen

† On leave from the Instituto de Investigaciones Fisicoquímicas Teóricas y Aplicadas (INIFTA), La Plata, Argentina.

(1) Clyne, M. A. A. *Symp. (Int.) Combust., [Proc.], 1962* **1963**, *9*, 211.
(2) Clyne, M. A. A.; Thrush, B. A. *Proc. R. Soc. London, Ser. A* **1963**, *275*, 559.
(3) Larkin, F. S.; Thrush, B. A. *Discuss. Faraday Soc.* **1964**, *37*, 112.
(4) Dodonov, A. F.; Lavrovskaya, G. K.; Talrose, V. L. *Kinet. Katal.* **1969**, *10*, 701.
(5) Westenberg, A. A.; Roscoe, J. M.; de Haas, N. *Chem. Phys. Lett.* **1970**, *7*, 597.
(6) Westenberg, A. A.; de Haas, N. *J. Phys. Chem.* **1972**, *76*, 1586.
(7) Hack, W.; Hoyermann, K. H.; Wagner, H. Gg. *Ber. Bunsenges. Phys. Chem.* **1978**, *82*, 713.
(8) Pratt, G. L.; Wood, S. W. *J. Chem. Soc., Faraday Trans. 1* **1983**, *79*, 2597.
(9) Bishop, W. P.; Dorfman, L. M. *J. Chem. Phys.* **1970**, *52*, 3210.
(10) Hikida, T.; Eyre, J. A.; Dorfman, L. M. *J. Chem. Phys.* **1971**, *54*, 3422.
(11) Nielsen, O. J.; Sillesen, A.; Luther, K.; Troe, J. *J. Phys. Chem.* **1982**, *86*, 2929.
(12) Burgess, R. H.; Robb, J. C. *Spec. Publ.—Chem. Soc.* **1957**, *No. 9*, 167.
(13) Burgess, R. H.; Robb, J. C. *Trans. Faraday Soc.* **1958**, *54*, 1008.
(14) Ahumada, J. J.; Michael, J. V.; Osborne, D. T. *J. Chem. Phys.* **1972**, *57*, 3736.
(15) Kurylo, M. J. *J. Phys. Chem.* **1972**, *76*, 3518.
(16) Wong, W.; Davis, D. D. *Int. J. Chem. Kinet.* **1974**, *6*, 401.
(17) Holstein, K. J.; Fink, E. H.; Wildt, J.; Winter, R.; Zabel, F. *J. Phys. Chem.* **1983**, *87*, 3943.
(18) Baulch, D. L.; Drysdale, D. B.; Horne, D. G.; Lloyd, A. C. "Evaluated Kinetic Data for High Temperature Reactions"; Butterworths: London, 1972; Vol. 1.
(19) Baulch, D. L.; Cox, R. A.; Hampson, R. F.; Kerr, J. A.; Troe, J.; Watson, R. T. *J. Phys. Chem. Ref. Data* **1980**, *9*, 295; *J. Phys. Chem. Ref. Data*, in press.
(20) Baulch, D. L.; Cox, R. A.; Crutzen, P. J.; Hampson, R. F.; Kerr, J. A.; Troe, J.; Watson, R. T. *J. Phys. Chem. Ref. Data* **1982**, *11*, 327.
(21) Kaufman; M.; Sherwell, J. *Prog. React. Kinet.* **1983**, *12*, 1.

0022-3654/85/2089-0342$01.50/0

isotope exchange in O + OH and the vibrational relaxation of O_2 in collisions with H. Given a reliable and complete HO_2 potential energy surface, one can simulate all these processes by trajectory calculations or by statistical theories of unimolecular reactions. For this reason, there has been a considerable effort to arrive at a reliable potential energy surface of HO_2. Ab initio calculations by Melius and Blint[22] lead to a barrier for the recombination (1) of 2.3 kcal mol^{-1}. Later ab initio calculations resulted in smaller barriers being $\lesssim$0.4 kcal mol^{-1} (ref 23 and 24) or in no barrier at all.[25] Because of its analytical representation, the Melius–Blint surface has been used for a series of trajectory calculations. However, also modified LEPS surfaces[26] and the empirical analytical surface from Murrell and co-workers[27] were employed for trajectory work. In particular, trajectory calculations have been used to study specific rate constants $k(E,J)$ for dissociation of excited HO_2 molecules,[28] cross sections for formation and stabilization of excited HO_2 species[29,30] in collisions of H and O_2, collisional energy transfer of excited HO_2 molecules,[30-32] and cross sections and product energy distributions for thermal and hot reactant conditions of reaction 2,[26,33-35] and, via microscopic reversibility, of reaction 3.

A careful comparison of the trajectory calculations of ref 33 with various forms of variational transition state theories for the thermal reaction 3 has been performed by Rai and Truhlar[36] (see also ref 37). It was shown in this work that the Melius–Blint ab initio surface obviously overestimates the long-range O–OH attraction whereas the Quack–Troe potential energy interpolation scheme[38] (as used in its most simple form[39]) leads to a much closer agreement with experimental results[37,40] on thermal rate coefficients of the reaction $O + OH \rightarrow H + O_2$. It appears most interesting also to compare different surfaces on the H–O_2 side of the HO_2 potential with the experimental results. Trajectory calculations[35] for the hot atom reaction $H + O_2 \rightarrow HO + O$, using the ab initio Melius–Blint surface, have led to markedly smaller total cross sections than observed experimentally.[41] So far, thermal rate coefficients of this reaction at high temperatures do not provide similarly conclusive results. It is the aim of our present work to provide a more detailed comparison of rate parameters for the H–O_2 side of the HO_2 surface, which were derived either by the use of the Melius–Blint surface or by the Quack–Troe interpolation scheme. As a result, we conclude that the Melius–Blint surface underestimates the long-range H–O_2 attraction in contrast to the overestimate of the long-range O–OH attraction whereas the Quack–Troe interpolation scheme works again very well.

A final part of the present work is concerned with energy-transfer properties of vibrationally highly excited HO_2 molecules. By an analysis[42,43] of limiting low-pressure rate coefficients, average energies $\langle \Delta E \rangle$ transferred per collision can be derived. These data then can be compared with recent trajectory calculations of the energy transfer of excited HO_2 molecules.[30-32]

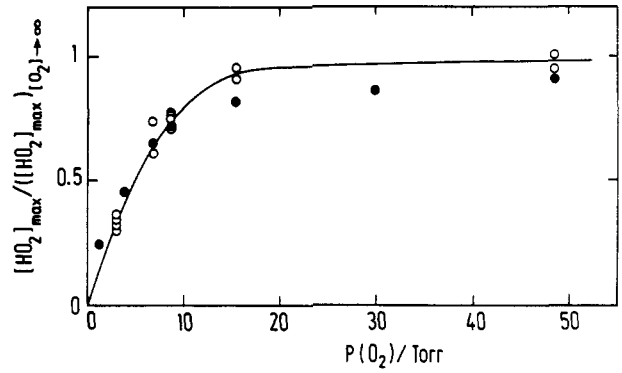

Figure 1. HO_2 maximum yields in the photolysis of $NH_3/O_2/N_2$ mixtures at $P(N_2)$ = 100 bar (○: experiments; ●: simulations with rate constants from Table II).

Experimental Technique and Evaluation

In our experiments H atoms were generated by laser flash photolysis of 1 torr of NH_3[44] using an ArF excimer laser (Lambda Physik EMG 200, 10-ns pulses of 100 mJ cm^{-2} at 193 nm). In the presence of O_2 (5–200 torr) and inert bath gases like Ar (1–170 bar), N_2 (1–200 bar), and CH_4 (1–10 bar), HO_2 is formed by reaction 1. We monitored HO_2 formation by its absorption near 220 nm.[45-48] The light source for absorption measurements was a Xe–Hg high-pressure arc lamp (Hanovia type 901 B, 200 W) whose intensity was increased by a factor of 500 by means of an electronic pulser. Absorption–time profiles were recorded by the use of a monochromator (Zeiss M4 QIII), photomultiplier (RCA 1P28), and oscilloscope (Tektronix 7633).

Our photolysis cell was made of stainless steel. It had cylindrical geometry (inner diameter 2 cm, height 2 cm). The cell was equipped with two sets of 20 mm thick quartz windows placed in the cell walls, perpendicularly to each other and to the axis of the cylinder. The laser-photolysis and lamp-probe beams traversed the cell through these windows at right angles. This arrangement allowed us to work under conditions where the dead volume was minimized; the light beams nevertheless had a minimum of wall contact, and laser stray light at the analysis side was negligible. A cell volume of about 2 cm^3 was irradiated by photolysis and probe light.

All experiments were performed near 298 K. The employed gases were all of commercially available high purity and were used without further purification. We employed NH_3 (Merck p.a., 99.99%), O_2 (Messer Griesheim, 99.996%), Ar (Messer Griesheim, 99.996%), N_2 (Messer Griesheim, 99.996%), and CH_4 (Merck p.a., 99.995%). No evidence for impurity effects was found.

The absorption signals observed after irradiation of $NH_3/O_2/N_2$ mixtures, from their spectral and kinetic properties, clearly could be identified as being due to HO_2 radicals. Experiments with O_2/N_2 mixtures in the absence of NH_3 (less than 200 torr of O_2) did not show O_3 absorption signals at 220 or 250 nm under our conditions. Also, there were no absorption signals at 220 nm after irradiation of NH_3/N_2 mixtures in the absence of O_2. In ex-

(22) Melius, C. F.; Blint, R. J. *Chem. Phys. Lett.* **1979**, *64*, 183.
(23) Dunning, T. H.; Walch, S. P.; Wagner, A. F. In "Potential Energy Surfaces and Dynamics Calculations for Chemical Reactions and Molecular Energy Transfer"; Truhlar, D. G., Ed.; Plenum Press: New York, 1981; p 329.
(24) Dunning, T. H.; Walch, S. P.; Goodgame, M. M. *J. Chem. Phys.* **1981**, *74*, 3482.
(25) Langhoff, S. R.; Jaffe, R. L. *J. Chem. Phys.* **1979**, *71*, 1475.
(26) Gauss, A. *J. Chem. Phys.* **1978**, *68*, 1689.
(27) Farantos, S.; Leisegang, E. C.; Murrell, J. N.; Texeira-Dias, J. J. C.; Varandas, A. J. C. *Mol. Phys.* **1977**, *34*, 947.
(28) Miller, J. A.; Brown, N. J. *J. Phys. Chem.* **1982**, *86*, 772.
(29) Blint, R. J. *J. Chem. Phys.* **1980**, *73*, 765.
(30) Gallucci, C. G.; Schatz, G. C. *J. Phys. Chem.* **1982**, *86*, 2352.
(31) Miller, J. A.; Brown, N. J. *Proc. Int. Symp. Gas Kinet., 7th* **1982**, 32.
(32) Miller, J. A.; Brown, N. J. *J. Chem. Phys.* **1984**, *80*, 5568.
(33) Miller, J. A. *J. Chem. Phys.* **1981**, *74*, 5120; **1981**, *75*, 5349.
(34) Bottomley, M.; Bradley, J. N.; Gilbert, J. R. *Int. J. Chem. Kinet.* **1981**, *13*, 957.
(35) Kleinermanns, K.; Schinke, R. *J. Chem. Phys.* **1984**, *80*, 1440.
(36) Rai, S. N.; Truhlar, D. G. *J. Chem. Phys.* **1983**, *79*, 6046.
(37) Howard, M. J.; Smith, I. W. M. *J. Chem. Soc., Faraday Trans. 2* **1981**, *77*, 997.
(38) Quack, M.; Troe, J. *Ber. Bunsenges. Phys. Chem.* **1974**, *78*, 240.
(39) Quack, M.; Troe, J. *Ber. Bunsenges. Phys. Chem.* **1977**, *81*, 329.
(40) Cohen, N.; Westberg, K. R. Aerospace Report No. ATR-82(7888)-3; Aerospace Co.: El Segundo, CA, 1982; *J. Phys. Chem. Ref. Data* **1983**, *12*, 531.
(41) Kleinermanns, K.; Wolfrum, J. *Laser Chem.* **1983**, *2*, 339; *J. Chem. Phys.* **1984**, *80*, 1446.
(42) Troe, J. *J. Chem. Phys.* **1977**, *66*, 4745, 4758.
(43) Troe, J. *J. Phys. Chem.* **1979**, *83*, 114.
(44) Okabe, H. "Photochemistry of Small Molecules"; Wiley: New York, 1978; p 269.
(45) Kijewski, H.; Troe, J. *Helv. Chim. Acta* **1972**, *55*, 205.
(46) Paukert, T. T.; Johnston, H. S. *J. Chem. Phys.* **1972**, *56*, 2824.
(47) Cox, R. A.; Burrows, J. P. *J. Phys. Chem.* **1979**, *83*, 2560.
(48) Sander, S. P.; Peterson, M.; Watson, R. T.; Patrick, R. *J. Phys. Chem.* **1982**, *86*, 1236.
(49) Troe, J. *Ber. Bunsenges. Phys. Chem.* **1969**, *73*, 906.
(50) Hippler, H.; Schippert, C.; Troe, J. *Int. J. Chem. Kinet. Symp.* **1975**, *1*, 27.
(51) van den Bergh, H.; Troe, J. *J. Chem. Phys.* **1976**, *64*, 736.
(52) Hippler, H.; Troe, J. *Int. J. Chem. Kinet.* **1976**, *8*, 501.
(53) Hippler, H.; Troe, J. *Ber. Bunsenges. Phys. Chem.* **1971**, *75*, 27.
(54) Croce de Cobos, A. E.; Troe, J. *Int. J. Chem. Kinet.*, in press.

periments with $NH_3/O_2/N_2$ mixtures, after the laser flash, the HO_2 signal initially increased linearly with time, before a maximum level was approached. The signal decayed on a much longer time scale such that formation and disappearance of HO_2 could easily be separated. The HO_2 concentrations were calibrated via the known HO_2 absorption coefficients[45-48] at 220 nm of $\epsilon = (1.0 \pm 0.1) \times 10^3$ L mol^{-1} cm^{-1}. The maximum HO_2 yields, obtained under high O_2 excess, corresponded to unit quantum yields of NH_3 photolysis into $H + NH_2$ and unit conversion of H atoms into HO_2.

With decreasing O_2 pressure, the HO_2 yields decreased. Figure 1 demonstrates the results of a study of HO_2 yields as a function of O_2 pressure for constant N_2 pressure of 100 bar. At small O_2 pressures the HO_2 yields increase with pressure until a maximum level is approached at pressures above 15 torr. Similar plots were determined for all bath gas pressures studied. However, at lower total gas pressures, higher oxygen pressures are required to approach the maximum HO_2 yield. E.g., at 1 bar of N_2, the maximum HO_2 yield is only obtained with more than 200 torr of added O_2. The investigations of the maximum HO_2 yields (before HO_2 signals decay again), such as documented in Figure 1, indicate complete conversion of H into HO_2 only at high excess of O_2. At lower O_2 pressures, a series of secondary reactions competes with reaction 1 such that lower HO_2 yields arise. The influence of these reactions can be understood, such as shown in the discussion below.

When HO_2 formation was studied under sufficiently large excess of O_2, pseudo-first-order conditions were established such that one could determine an effective rate coefficient for HO_2 formation via the relation

$$[HO_2] \simeq [HO_2]_{max}(1 - \exp(-k_f[O_2]t)) \quad (4)$$

Unfortunately, under these conditions, HO_2 formation often became so fast that it interfered with the laser flash. For this reason it appeared more reasonable to work with oxygen pressures slightly below the range where the maximum HO_2 yields are achieved. We generally chose conditions for which the HO_2 yield was 80% of the maximum yield. For these conditions, experimentally no deviations from eq 4 could be recognized as yet. However, in order to obtain k_1 from k_f, we had to correct by multiplying the apparent first-order rate coefficient from eq 4 by the reduction factor of the yield $[HO_2]_{max}/([HO_2]_{max})_{[O_2]\to\infty}$; see the discussion of the mechanism given below. Alternatively, we derived k_1 directly from the initial rate of HO_2 formation which was calibrated via the maximum possible HO_2 yield in large excess of O_2, or via the HO_2 absorption coefficient and the number of absorbed photons. All methods gave identical results.

After having reached its maximum (generally on a 10–100-ns time scale), the HO_2 absorption signal decayed on a 10–100-μs time scale following second-order kinetics. The phenomenological second-order decay coefficient k_d, defined by

$$[HO_2]^{-1} - [HO_2]_{max}^{-1} = k_d(t - t_{max}) \quad (5)$$

turned out to be independent of the O_2 and total gas pressures. Similarly, as the phenomenological pseudo-first-order rate coefficients of HO_2 formation, the second-order rate coefficients for HO_2 disappearance have to be interpreted by a series of bimolecular reactions. These are discussed below.

Results

The main experimental observables of our work were the HO_2 maximum yields, the phenomenological pseudo-first-order rate coefficients of HO_2 formation, k_f, and the phenomenological second-order rate coefficients of HO_2 disappearance k_d. The dependence of these observables on the pressure of added O_2, on the total gas pressure, and on the nature of the added inert gas was studied over wide ranges of conditions. A simulation of the mechanism (see below) indicated that k_1 either follows directly from the initial rate of HO_2 formation or follows from k_f via

$$k_1 \simeq k_f[HO_2]_{max}/([HO_2]_{max})_{[O_2]\to\infty} \quad (6)$$

k_1 values obtained in this way from the two methods are summarized in Table I for the bath gases Ar, N_2, and CH_4. Each value is the average of 8–16 measurements. The results are illustrated in Figures 2–4. The uncertainty of the shown points,

TABLE I: Rate Coefficients k_1 for the Reaction $H + O_2 (+M) \to HO_2 (+M)$ at 298 K

$P(O_2)^a$/torr	P(M)/bar	$k_1/(10^{-11}$ cm^3 molecule^{-1} s^{-1})
	M = N_2	
200	1	0.12
160	2	0.21
60	5	0.48
60	10	0.62
20	25	1.4
20	50	1.9
10	100	3.3
10	200	3.9
	M = Ar	
200	1	0.061[b]
100	2	0.091[c]
80	5	0.23
30	10	0.39
20	25	0.64
20	50	1.2
10	100	1.7
10	170	2.3
	M = CH_4	
60	1	0.26
30	2	0.49
15	5	0.91
10	10	1.4

[a] O_2 pressures of most experiments, corresponding to $k_1 \simeq 0.8k_f$. [b] Corrected for contribution from M = O_2, uncorrected value = 0.083. [c] Corrected for contribution from M = O_2, uncorrected value = 0.12.

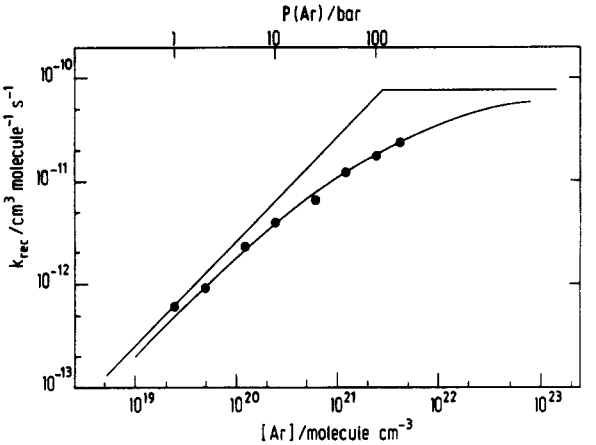

Figure 2. Rate coefficients for the recombination $H + O_2 (+M) \to HO_2 (+M)$, bath gas M = Ar.

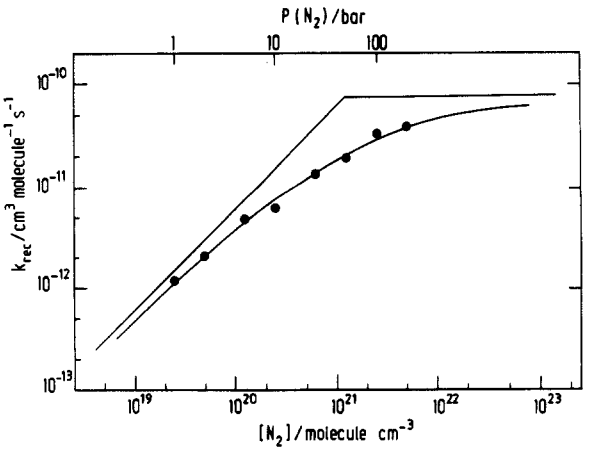

Figure 3. Rate coefficients for the recombination $H + O_2 (+M) \to HO_2 (+M)$, bath gas M = N_2.

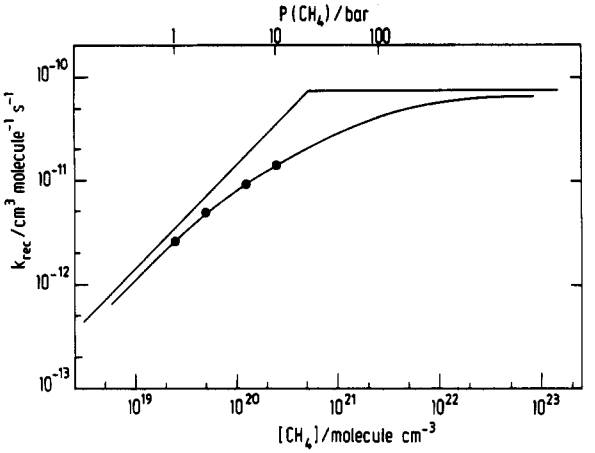

Figure 4. Rate coefficients for the recombination H + O_2 (+M) → HO_2 (+M), bath gas M = CH_4.

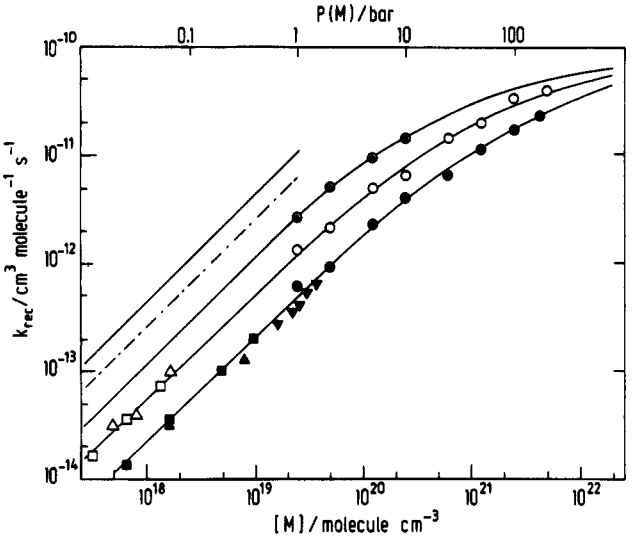

Figure 5. Rate coefficients for the recombination H + O_2 (+M) → HO_2 (+M). M = Ar: ● = this work, ▼ = ref 10, ▲ = ref 15, ■ = ref 16; M = N_2: ○ = this work, △ = ref 15, □ = ref 16; M = CH_4: ⊙ = this work; ···: ref 15; —: ref 16.

due to the scatter and the corrections indicated in eq 6, is estimated to be about ±30%. The points show the typical behavior of a recombination reaction in the falloff range. We extrapolated the falloff curves to the limiting low- and high-pressure rate coefficients by the use of the theoretical models described below. These constructions lead to the full curves and limits of the rate coefficients shown in the figures. One should note that the two lowest points for the bath gas Ar had to be corrected for the collision efficiency of the added O_2 which is different from that of Ar.

Our measurements near to the low-pressure limit well confirm earlier measurements in Ar and N_2. Figure 5 compares our data with results from the literature which were all obtained at pressures below 1.5 bar. Our results do confirm the marked difference between the low-pressure rate coefficients in the bath gases Ar and N_2 which was observed in ref 15 and 16. However, for the bath gas CH_4, we observed a smaller rate coefficient than expected from earlier results which were, however, obtained at lower pressures.

By means of the construction of the falloff curve discussed below the following limiting low-pressure rate coefficients were derived

$$k_{rec,0} = [Ar](2.8 \times 10^{-32}) \text{ cm}^6 \text{ molecule}^{-2} \text{ s}^{-1}$$

$$k_{rec,0} = [N_2](6.5 \times 10^{-32}) \text{ cm}^6 \text{ molecule}^{-2} \text{ s}^{-1}$$

$$k_{rec,0} = [CH_4](1.5 \times 10^{-31}) \text{ cm}^6 \text{ molecule}^{-2} \text{ s}^{-1}$$

for the bath gases Ar, N_2, and CH_4, respectively. For all three bath gases the same value for the limiting high-pressure rate coefficient of

$$k_{rec,\infty} = 7.5 \times 10^{-11} \text{ cm}^3 \text{ molecule}^{-1} \text{ s}^{-1}$$

was derived. The estimated uncertainty of $k_{rec,0}$ because of scatter of the data and uncertainty of the evaluation, in particular of the effects of secondary reactions, is about ±15% for Ar and N_2. The estimated uncertainty of $k_{rec,\infty}$ because of the same reasons and, in addition, of the uncertainty of the falloff extrapolation, is about ±25%. An approach of k_∞ to within 20% would have required experiments with total gas pressures of the order of 2000 bar. Although we have performed laser flash photolysis experiments up to gas pressures of 7000 bar in our laboratory,[55] we did not apply this difficult technique to the present system. In view of the reliability of the falloff extrapolation technique such as demonstrated, e.g., by the recent experiments on the reaction NO_2 + NO_3 → N_2O_5,[56] the presently applied pressure range was considered sufficient for a determination of k_∞. The measurements with the bath gas CH_4 give much less reliable limiting rate coefficients since only a factor of 10 variation in pressure was applied in contrast to the factor of 100 for Ar and N_2.

TABLE II: Rate Coefficients k_d from Eq 5 for Decay of HO_2[a]

$P(O_2)$/torr	$P(N_2)$/bar	$k_d/(10^{-11}$ cm^3 molecule^{-1} s^{-1}) exptl	calcd
150	1	6.1	7.2
100	5	5.2	5.9
14	10	5.1	6.5
30		5.6	6.5
59		4.5	5.8
86		6.6	5.5
6.8	100	9.0	6.6
8.6		6.6	5.9
8.7		7.3	5.9
0.9	200	7.0	7.9
2.2		8.0	6.7
4.8		9.6	6.3
6.9		4.7	6.2
9.0		6.9	6.0
9.7		8.3	5.9
21		6.8	5.4
21		8.3	5.4

[a] Calculations with k_1 from this work; $k_7 = 6.4 \times 10^{-12}$ and $k_9 = 1.1 \times 10^{-10}$ cm^3 molecule^{-1} s^{-1} from ref 19 and 20; $k_{10} = 5 \times 10^{-12}$ (1 bar, ref 72), $k_{10} = 8 \times 10^{-12}$ (estimate for 200 bar, maximum value compatible with k_d), $k_{11} = 3.5 \times 10^{-11}$, $k_{12} = 1.6 \times 10^{-11}$ (estimate, $k_{11} + k_{12}$ from ref 73), $k_{13} = 5 \times 10^{-11}$ (estimate), $k_{14} = 5 \times 10^{-11}$ (estimate), and $k_{15} = 5 \times 10^{-11}$ cm^3 molecule^{-1} s^{-1} (estimate).

Table II summarizes our measurements of the phenomenological second-order rate coefficient k_d of HO_2 disappearance. Within the scatter of the data, no systematic dependence of k_d on O_2 or N_2 pressures can be detected. An average of all values is given by

$$k_d = (6.8 \pm 1.5) \times 10^{-11} \text{ cm}^3 \text{ molecule}^{-1} \text{ s}^{-1}$$

The interpretation of k_d in terms of rate constants of elementary reactions involved is less direct than for k_f. An analysis of the mechanism of HO_2-consuming reactions is given below. Our results on the maximum HO_2 yields, such as demonstrated in Figure 1, are as well analyzed below in terms of the reaction mechanism involved.

Discussion

Reaction Mechanism. The primary photolysis of NH_3 at 193 nm is known to produce H + $NH_2(\tilde{X}^2B_1)$ with a quantum yield near unity.[44] Our experiments with total gas pressures up to 200 bar showed no indication of a reduction of the quantum yield with increasing pressure.

(55) Hippler, H.; Schubert, V.; Troe, J. *J. Chem. Phys.* **1984**, *81*, 3931.
(56) Croce de Cobos, A. E.; Hippler, H.; Troe, J. *J. Phys. Chem.* **1984**, *88*, 5083.

Under sufficiently high excess of O_2 over NH_3, hydrogen atoms exclusively add to oxygen to form HO_2 radicals via

$$H + O_2 + M \rightarrow HO_2 + M \quad (1)$$

such that k_f, as defined by eq 4, is equal to the pseudo-second-order rate coefficient k_1 of reaction 1. Most probably NH_2 radicals, even at 200 bar, do not add to O_2 forming NH_2O_2 radicals.[20]

If the O_2 pressure is not high enough such that reaction 1 is comparably slow, hydrogen atoms attack HO_2 via

$$H + HO_2 \rightarrow HO + HO \quad (7)$$

$$\rightarrow H_2 + O_2 \quad (8)$$

$$HO + HO_2 \rightarrow H_2O + O_2 \quad (9)$$

Recombination of hydrogen atoms with NH_2 or bimolecular reactions of H or OH with NH_3 are too slow under our conditions to interfere with the given mechanism. The result of reactions 7–9 is a reduction of the HO_2 yield compared to the maximum yield, obtained for sufficiently high excess of O_2 with reaction 1 only. Numerical integration of the rate equations with rate constants from the CODATA compilation[19,20] leads to the points included in Figure 1. Obviously the observed HO_2 yields are in agreement with this simulation. This result was also obtained for all the other conditions. The simulation also confirms the validity of the conversion from k_f to k_1 via eq 6.

Under sufficiently high excess of O_2, at the end of the short period of HO_2 formation only HO_2 and NH_2 radicals are present, which on a much slower time scale can react via the following mechanism:

$$HO_2 + HO_2 \rightarrow H_2O_2 + O_2 \quad (10)$$

$$HO_2 + NH_2 \rightarrow NH_3 + O_2 \quad (11)$$

$$\rightarrow HNO + H_2O \quad (12)$$

$$HNO + HO_2 \rightarrow H_2O_2 + NO \quad (13)$$

$$\rightarrow H_2O + NO_2 \quad (14)$$

$$HNO + NH_2 \rightarrow NH_3 + NO \quad (15)$$

In addition, reactions between NH_2 radicals and reactions with secondary products occur. With literature values (see Table II) for the rate constants (and some estimates for side reactions), the simulation of the whole mechanism leads to values for the phenomenological rate coefficients k_d of HO_2 disappearance which are included in Table II. The very weak dependences of k_d on the O_2 pressure and the total gas pressure are smaller than the experimental scatter. The average of the simulated k_d values of $k_d = (6.2 \pm 0.7) \times 10^{-11}$ cm^3 molecule^{-1} s^{-1} agrees well with the average experimental value. The simulation shows that at sufficiently large O_2 excess, reactions 10–12 are dominantly responsible for the HO_2 decay with minor contributions from reactions 13–15. It is, however, not possible to derive separate information on the individual rate constants k_{10}, k_{11}, and k_{12} from the measured k_d values.

Analysis of H + O_2 Recombination Rate Coefficients. Our experimental k_1 values have to be analyzed in terms of unimolecular rate theory. In practice, this analysis involves a preliminary construction of reduced falloff curves, an extrapolation of the measured rate coefficients with these falloff curves toward limiting low- and high-pressure rate coefficients, a theoretical interpretation of the limiting rate coefficients leading to a refined construction of the falloff curves, and a final fit. This procedure has also been followed in the present work. In the following we give an interpretation of the final results.

Limiting High-Pressure Rate Coefficients. We interpret the derived $k_{rec,\infty}$ values in terms of the simplified version of the statistical adiabatic channel model, which was proposed in its canonical form in ref 57 and in its microcanonical form in ref 58. According to ref 57, one has

$$k_{rec,\infty} = K_c^{-1} k_{diss,\infty}$$

$$= K_c^{-1} \frac{kTQ^*_{cent}F^*_{AM}\prod_r^r Q^*_j \prod_b^b Q^*_m}{h\sigma^* Q_{vib}Q_{rot}} \exp\left(-\frac{\Delta H_0^\circ + \Delta E_{OZ}}{kT}\right) \quad (16)$$

In this equation, K_c denotes the equilibrium constant $([H][O_2]/[HO_2])_{eq}$, $k_{diss,\infty}$ the limiting high-pressure rate coefficient of HO_2 dissociation, Q^*_{cent} the centrifugal pseudopartition function, F^*_{AM} an angular momentum coupling correction factor, σ^* an effective symmetry number, Q^*_j the pseudopartition functions of the r conserved oscillators of HO_2, and Q^*_m the pseudopartition functions of the b disappearing oscillators of HO_2 transforming into product rotors. Q_{vib} and Q_{rot} are vibrational and rotational partition functions of HO_2, ΔH_0° is the reaction enthalpy at 0 K, and ΔE_{OZ} is the energy barrier of the lowest reaction channel in coming from the recombination side. With the relationships from ref 57, the factors in eq 16 are easily calculated as a function of the ratio α/β between the looseness parameter α and the Morse parameter β. With the fitted value

$$\alpha = 0.94 \text{ Å}^{-1}$$

and the calculated $\beta = 2.94$ Å^{-1} (from the force constant 6.502 mdyn Å^{-1} of the H–O_2 bond[27,59]), the experimental value $k_{rec,\infty} = 7.5 \times 10^{-11}$ cm^3 molecule^{-1} s^{-1} is reproduced. The derived looseness parameter $\alpha = 0.94$ Å^{-1} of the HO_2 potential energy surface, within the uncertainty of ±0.1 Å^{-1}, is identical with the "standard value" $\alpha \simeq 1$ Å^{-1} which we obtained[38,39] from an analysis of several reaction systems.

Once the α value is fixed by a fit to one experimental quantity, other quantities can be predicted. In particular, the temperature dependence of $k_{rec,\infty}$ over the range 200–400 K with eq 16 is calculated to be

$$k_{rec,\infty} \simeq 7.5 \times 10^{-11}(T/300 \text{ K})^{0.6} \text{ cm}^3 \text{ molecule}^{-1} \text{ s}^{-1}$$

Other quantities to be predicted are discussed below.

Limiting Low-Pressure Rate Coefficients. The derived $k_{rec,0}$ values are analyzed in terms of the factorized expression

$$k_{rec,0}/[M] \simeq K_c^{-1}\beta_c Z_{LJ} \frac{\rho_{vib,h}(E_0)kT}{Q_{vib}} \exp\left(-\frac{\Delta H_0^\circ + \Delta E_{OZ}}{kT}\right) F_{anh}F_E F_{rot} \quad (17)$$

from ref 42 and 43. The various factors are evaluated with the HO_2 vibrational frequencies[59] 3436, 1392, and 1098 cm^{-1}, the O_2 frequency of 1580 cm^{-1}, the HO_2 rotational constants[60] $A = 20.4$, $B = 1.12$, and $C = 1.06$ cm^{-1}, and the reaction enthalpy[21,61] $\Delta H_0^\circ = 201.25$ kJ mol^{-1}. Lennard-Jones collision frequencies Z_{LJ} are calculated with the parameters $\sigma = 4.2$ Å and $\epsilon/k = 289$ K for HO_2 (as[42] for H_2O_2), and $\sigma = 3.5$, 3.7, 3.8 Å and $\epsilon/k = 114$, 82, 142 K for Ar, N_2, and CH_4, respectively.[62] In order to calculate the rotational factor F_{rot}, it is very important to employ a realistic radial dependence of the H–O_2 potential and an adequate centrifugal potential. The most simple van der Waals expression for the H–O_2 potential combined with a quasi-diatomic centrifugal potential[42] leads to $F_{rot}(298 \text{ K}) = 42$, whereas the much more realistic Morse interaction potential together with a triatomic centrifugal potential[43] leads to $F_{rot}(298 \text{ K}) = 9.1$. The latter approach was chosen here. By a comparison of the strong collision rate coefficients ($\beta_c = 1$) with the experimental values of $k_{rec,0}$, the following values of the collision efficiencies β_c are derived: $\beta_c(Ar) = 0.14$, $\beta_c(N_2) = 0.29$, and $\beta_c(CH_4) = 0.52$. These experimental values, via the relationship[42]

$$\frac{\beta_c}{1 - \beta_c^{1/2}} \simeq \frac{-\langle \Delta E \rangle}{F_E kT} \quad (18)$$

(57) Troe, J. *J. Chem. Phys.* **1981**, *75*, 226.
(58) Troe, J. *J. Chem. Phys.* **1983**, *79*, 6017.
(59) (a) Yamada, C.; Endo, Y.; Hirota, E., presented in part at the 43rd Annual Meeting of the Chemical Society of Japan, Tokyo, 1981. (b) Nagai, K.; Endo; Y.; Hirota, E. *J. Mol. Spectrosc.* **1981**, *89*, 520. (c) Johns, J. W. C.; McKellar, A. R. W.; Riggin, M. *J. Chem. Phys.* **1978**, *68*, 3957.
(60) Charo, A.; De Lucia, F. C. *J. Mol. Spewctrosc.* **1982**, *94*, 426.
(61) Shum, L. G. S.; Benson, S. W. *J. Phys. Chem.* **1983**, *87*, 3479.
(62) Mourits, F. M.; Rummens, F. H. A. *Can. J. Chem.* **1977**, *55*, 3007.

TABLE III: Analysis of Low-Pressure Rate Coefficients $k_{rec,0}$ of $H + O_2$ (+M) → HO_2 (+M)

T/K	M	$k_{rec,0}$/([M](10^{-32}) cm^6 molecule^{-2} s^{-1})	β_c	$-\langle\Delta E\rangle$/(kJ mol^{-1})
298	He	2.5[a]	0.091	0.33
1000		0.68[b]	0.023	0.24
298	Ar	2.8[c]	0.14	0.57
1000		0.69[d]	0.032	0.35
298	H_2	6.0[e]	0.12	0.46
1000		1.7[f]	0.032	0.35
298	N_2	6.5[c]	0.29	1.6
1000		1.0[g]	0.041	0.46
298	O_2	5.9[h]	0.28	1.5
1900		0.21[i]	0.013	0.26
298	CH_4	15[c]	0.52	4.7

[a] Experimental value from ref 7. [b] Experimental value from ref 18. [c] Experimental value from this work. [d] Experimental value from ref 19. [e] Experimental value from ref 11. [f] Experimental value from ref 74. [g] Experimental value from ref 75. [h] Experimental value from ref 20. [i] Experimental value from ref 76.

allow one to obtain average energies $\langle\Delta E\rangle$ transferred per collision. One derives in this way $\langle\Delta E\rangle \simeq -0.6$ kJ mol^{-1} for M = Ar, −1.6 kJ mol^{-1} for M = N_2, and −4.7 kJ mol^{-1} for M = CH_4. It should be emphasized that the uncertainties of the experiments and of the theoretical analysis leave an uncertainty of probably a factor of 2 in these $\langle\Delta E\rangle$ values. However, the order of magnitude agrees very well with the data for related systems[42,43] and with recent direct measurements in highly excited CS_2[63] and SO_2[64] molecules.

Equations 17 and 18 also allow one to analyze the temperature coefficient of $k_{rec,0}$. In Table III we summarize experimental values of $k_{rec,0}$, and the derived β_c and $\langle\Delta E\rangle$ values for the bath gases He, Ar, H_2, N_2, and O_2 at 298 and 1000 (or 1900) K. Very marked decreases of β_c with increasing temperature are noticed which are in accord with only slightly decreasing values of $-\langle\Delta E\rangle$. Only for N_2 and O_2 are marked decreases of $-\langle\Delta E\rangle$ found. One has to ask how much of these effects are outside the experimental errors. It will be interesting to compare these results with our forthcoming experiments on the temperature coefficients of directly measured $\langle\Delta E\rangle$ in excited CS_2 and SO_2.[65] Recent results[66] on directly measured $\langle\Delta E\rangle$ in excited toluene molecules indicated only small negative temperature coefficients of $\langle\Delta E\rangle$.

Intermediate Falloff Curves. Following the concepts of ref 43, 67, and 68, the transition of k_{rec} from $k_{rec,0}$ to $k_{rec,\infty}$ is represented by reduced falloff curves

$$\frac{k_{rec}}{k_{rec,\infty}} = \left(\frac{k_{rec,0}/k_{rec,\infty}}{1 + k_{rec,0}/k_{rec,\infty}}\right) F^{SC}(k_{rec,0}/k_{rec,\infty}) F^{WC}(k_{rec,0}/k_{rec,\infty}) \quad (19)$$

The analogous expression would apply for dissociation rate coefficients. The strong collision broadening factors F^{SC}, depending on the "reduced pressure scale" $k_{rec,0}/k_{rec,\infty}$, are expressed by the empirical relationships from ref 43 and 67 which were derived from rigid RRKM theory. These relations use the parameters S_K and B_K

$$S_K = 1 - \frac{1}{T}\frac{\partial \ln Q^*}{\partial(1/T)} \quad (20)$$

$$B_K = \frac{S_K - 1}{s - 1}\left(\frac{E_0 + a(E_0)E_z}{kT}\right) \quad (21)$$

(63) Dove, J. E.; Hippler, H.; Troe, J. *J. Chem. Phys.*, in press.
(64) Hippler, H.; Nahr, D.; Troe, J., to be submitted for publication.
(65) Heymann, M.; Hippler, H.; Troe, J., to be submitted for publication.
(66) Heymann, M.; Hippler, H.; Troe, J. *J. Chem. Phys.* **1984**, *80*, 1853.
(67) Troe, J. *Ber. Bunsenges. Phys. Chem.* **1983**, *87*, 161.
(68) Gilbert, R. G.; Luther, K.; Troe, J. *Ber. Bunsenges. Phys. Chem.* **1983**, *87*, 169.

TABLE IV: Specific Rate Constants $k(E,J)$ for Dissociation of HO_2[a]

$(E - E_0(J=0))$/(kJ mol^{-1})	$k(E,J)$/(10^{12} s^{-1})	$(E - E_0(J=0))$/(kJ mol^{-1})	$k(E,J)$/(10^{12} s^{-1})
$J = 0$		20	1.77
0	0.36	25	1.95
2.5	0.62	30	2.44
5	0.78	35	2.85
7.5	0.89	40	3.26
10	0.99	45	3.60
15	1.14	50	4.03
20	1.30	55	4.31
25	1.55	60	4.85
30	1.77	$J = 33$	
35	1.94	8.9	0.022
40	2.15	15	0.59
45	2.37	20	0.91
50	2.56	25	1.35
55	2.68	30	1.67
60	2.81	35	2.28
65	2.95	40	2.74
$J = 10$		45	3.26
0.8	0.036	50	3.97
2.5	0.18	55	4.40
5	0.42	60	4.91
7.5	0.74		
10	1.00		
15	1.28		

[a] Simplified statistical adiabatic channel calculations[58] with $\alpha = 0.94$ Å^{-1}.

where the "activated complex partition function" Q^* is given from the formal expression for the dissociation rate constant at high pressures $k_{diss,\infty}$ by

$$k_{diss,\infty} = \frac{kT}{h}\frac{Q^*}{Q_{vib}Q_{rot}}\exp\left(-\frac{E_0}{kT}\right) \quad (22)$$

s is the number of oscillators of the dissociating molecule, E_z its zero-point energy, E_0 its dissociation energy at 0 K, and $a(E_0)$ the Whitten–Rabinovitch correction factor. It should be emphasized that detailed falloff curves so far never have been calculated for simple bond fission reactions, like the present reaction system, taking into account specific rate constants $k(E,J)$ which properly obey conservation of angular momentum. It appears, however, very reasonable to apply our concept of reduced falloff curves also to these cases, by determining S_K from the proper expression for $k_{diss,\infty}$ accounting for angular momentum effects. Equation 16 fulfills this requirement. Therefore, we have calculated S_K from the above given temperature dependence of $k_{rec,\infty}$ (after a conversion into $k_{diss,\infty}$). In this way, $S_K = 3.16$ and $B_K = 103$ are obtained for 298 K.

Besides the strong collision broadening factors F^{SC}, the weak collision broadening factors F^{WC} from ref 43 and 68 are calculated in order to account for the broadening of falloff curves because of weak collision effects. The final results of our construction of reduced falloff curves at 298 K can be expressed approximately by

$$\log F^{SC}F^{WC} \simeq \left[1 + \left(\frac{\log(k_{rec,0}/k_{rec,\infty})}{N}\right)^2\right]^{-1} \log F_{cent} \quad (23)$$

with broadening factors at the center of the falloff curves $F_{cent} \simeq 0.45$, 0.50, and 0.54 and widths of the falloff curves $N \simeq 1.19$, 1.13, and 1.09 for M = Ar, N_2, and CH_4, respectively. F_{cent} and N are calculated by the empirical techniques of ref 43, 67, and 68.

Specific Rate Constants $k(E,J)$ for Dissociation of HO_2. After the looseness parameter α of the HO_2 potential energy surface has been fixed via a comparison of the $k_{rec,\infty}$ expression of eq 16 to the experiments, we employ the microcanonical simplified version of the statistical adiabatic channel model of ref 58, in order

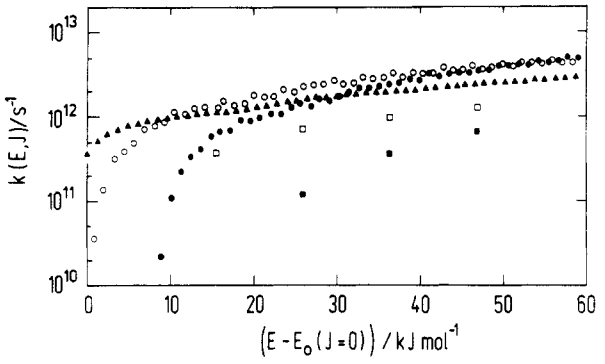

Figure 6. Specific rate constants $k(E,J)$ for the dissociation of $HO_2 \rightarrow H + O_2$. This work: calculations by simplified statistical adiabatic channel model[58] with $\alpha = 0.94$ Å^{-1} for $J = 0$ (▲), $J = 10$ (○), and $J = 33$ (●). Trajectory calculations from ref 28 using the Melius–Blint ab initio surface[22] for "$J \leq 10$" (□) and "$30 \leq J \leq 35$" (■).

to construct a set of specific rate constants $k(E,J)$ for dissociation of excited HO_2 molecules. Our results can to some extent be compared with various trajectory calculations in ref 28–30 which used the Melius–Blint ab initio surface. It appears most interesting to compare these results with our specific rate constants which are based on a different potential energy model.

Figure 6 and Table IV give statistically calculated specific rate constants for $J = 0$, 10, and 33 based on the α value of 0.94 Å^{-1}. One notices the same general features as observed and explained in earlier calculations of $k(E,J)$ for NO_2, C_2H_6,[58] H_2CO, and D_2CO:[69] At energies near to the threshold energies for dissociation, $k(E,J)$ decreases with increasing J, whereas at higher energies the curves for different J values merge and finally cross. We would like to mention that we have also averaged our $k(E,J)$ curves over a thermal distribution of total energies E (rotational plus vibrational energy) and of total angular momenta J. The result for 298 K was $k_{rec,\infty} = 8.7 \times 10^{-11}$ cm^3 molecule^{-1} s^{-1}, in close agreement with the experimental value 7.5×10^{-11} cm^3 molecule^{-1} s^{-1} on which the determination of α was based. The microcanonical and canonical versions of the theory are not completely equivalent such that the small discrepancy can be due either to numerical uncertainties (graining) or to small differences between the two versions of the theory.

In Figure 6 we compare our statistical calculations of $k(E,J)$ with trajectory calculations by Miller and Brown[28] performed on the Melius–Blint ab initio surface. In order to do this comparison, we proceed in the following way: The Melius–Blint surface shows a 2.3 kcal mol^{-1} exit barrier for dissociation of HO_2. This would contribute a Boltzmann factor of $\exp(-2.3 \text{ kcal mol}^{-1}/RT) = 0.02$ to $k_{rec,\infty}$ at 298 K. The high experimental value of $k_{rec,\infty}$ rules out the existence of this barrier, which was also not observed in later ab initio calculations.[23-25] For this reason and in order not to be misled by the too small HO_2 dissociation energy of the ab initio surface, we have chosen a representation of $k(E,J)$ as a function of the excess energy $E - E_0(J=0)$ above the lowest dissociation threshold energy at $J = 0$. Miller and Brown[28] did calculations for "$J \leq 10$" and "$30 \leq J \leq 35$". Figure 6 shows that, for the two J values, their results for small excess energies $E - E_0(J)$ appear to extrapolate toward our threshold rate constants. This is not surprising since the threshold rate constants $k(E_0(J)) = 1/h\rho(E_0(J))$ only depend on the threshold energies $E_0(J)$ and not on other details of the potential surface. However, at energies larger than the threshold energies the Melius–Blint surface produces $k(E,J)$ values markedly below our results. This behavior obviously has to be attributed to the much more "rigid" character of the surface when an exit barrier "contracts" the outgoing potential valley. A thermal rate coefficient $k_{rec,\infty}$ calculated with $k(E,J)$ from the Melius–Blint surface would, therefore, be by orders of magnitude smaller than the experiments, a factor of 50 because of the Boltzmann factor and an additional large factor because of the rigidity of the surface.

(69) Troe, J. *J. Phys. Chem.* **1984**, *88*, 4375.

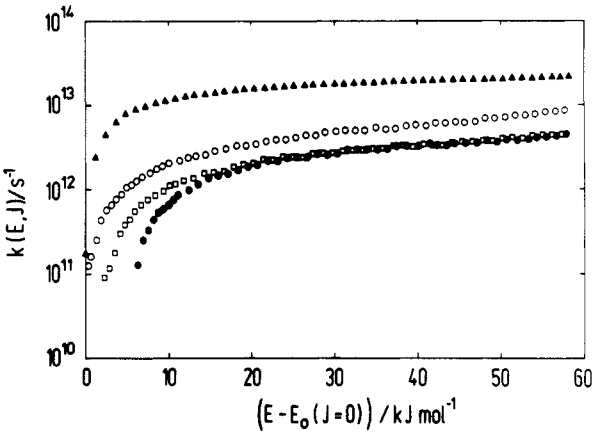

Figure 7. Specific rate coefficients $k(E,J)$ for the dissociation $HO_2 \rightarrow HO + O$. Calculations for $J = 0$ (▲), 10 (○), 40 (□), and 60 (●).

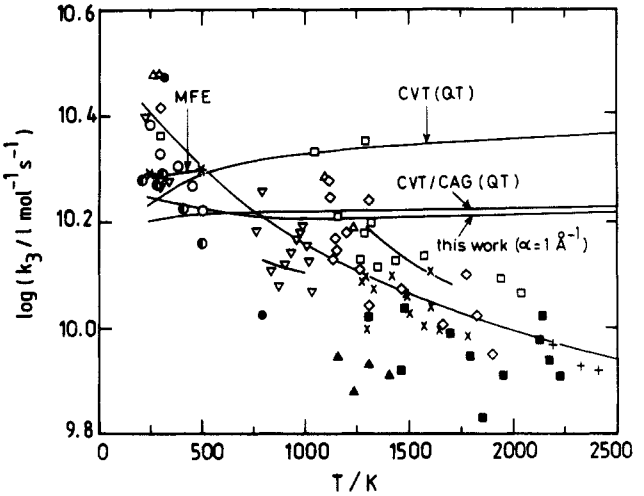

Figure 8. Rate constants k_3 for the reaction $HO + O \rightarrow H + O_2$. (Experiments: ◐, ref 71; ○, ref 37; all other experimental points and unlabeled curves from data compilation in ref 40. Calculations: *—* (MFE), maximum free energy calculation[39] from ref 37; CVT(QT), canonical variational theory from ref 36; CVT/CAG(QT), canonical variational theory with transmission coefficient from ref 36; MFE, CVT, and CVT/CAG with Quack–Troe interpolation scheme[39] using $\gamma = 0.75$ Å^{-1}; this work, simplified statistical adiabatic channel calculation[57] with $\alpha = 1$ Å^{-1}.

Comparison with Trajectory Calculations and Experiments on the Reactions $H + O_2 \rightleftharpoons HO + O$. Whereas the Melius–Blint surface at the $H + O_2$ side has the defect of a barrier and, related with it, of a too rigid character, on the $HO + O$ side it shows a too strong attraction.[36] This conclusion was derived by Rai and Truhlar from a comparison with experimental results on the thermal rate constant of reaction 3. These authors also applied variational transition state theory using the Quack–Troe interpolation scheme with a standard value for the partition function interpolation parameter $\gamma = 0.75$ Å^{-1} which corresponds to $\alpha = 1$ Å^{-1}. We have redone this calculation for reaction 3, $HO + O \rightarrow H + O_2$, with the statistical adiabatic channel model for $\alpha = 1$ Å^{-1}. At first, we have calculated the specific rate constants $k(E,J)$ for the dissociation channel $HO_2 \rightarrow HO + O$. Our results are shown in Figure 7. Quite different from the $HO_2 \rightarrow H + O_2$ channel illustrated in Figure 6, the $k(E,J)$ curves for different J values do not cross in the shown energy range. This can be understood by the different moments of inertia of the fragments: reaction in the $HO + O$ channel corresponds nearly to a quasi-diatomic fragmentation of HO_2 where the K-rotor does contribute much less than for the $H + O_2$ channel. With the markedly different orders of magnitude of the $k(E,J)$ for the $H + O_2$ and $HO + O$ channels, one can safely assume that k_3 is nearly equal to the high-pressure recombination rate coefficient $k_{rec,\infty}$ of a process $HO + O \rightarrow HO_2$. Figure 8 shows our results derived with eq 16 from 300 up to 2500 K (see also Table V) in comparison

TABLE V: Simplified Statistical Adiabatic Channel Calculations[57] of k_3 for the Reaction $O + OH \rightarrow O_2 + H$[a]

T/K	$k_3/(10^{-11}$ cm^3 molecule^{-1} s^{-1})	T/K	$k_3/(10^{-11}$ cm^3 molecule^{-1} s^{-1})
300	2.88	1500	2.69
500	2.81	2000	2.74
750	2.69	2500	2.75
1000	2.63		

[a] Using $\alpha = 1$ Å^{-1}.

with Rai and Truhlar's variational transition state calculations, with a maximum free energy calculation[39] by Howard and Smith[37] using $\gamma = 0.75$ Å^{-1}, and with experimental data.[40] Within minor differences, the statistical calculations are equivalent. We therefore predict a nearly temperature-independent value of k_3 over the temperature range 250–3000 K of

$$k_3 \simeq 2.8 \times 10^{-11} \text{ cm}^3 \text{ molecule}^{-1} \text{ s}^{-1}$$

(Including back-dissociation $HO_2^* \rightarrow HO + O$, one would obtain a 5% smaller value.) It appears highly satisfactory that our statistical prediction agrees with all the experimental data at least within about a factor of 2. It should be emphasized that this prediction apart from using the standard α value employs no adjustable parameters. Nevertheless, the comparison of our predicted value of k_3 with the experiments shows a marked discrepancy in the temperature coefficients. If our prediction is right, the majority of the high-temperature data would have to be too low by about a factor of 2. Very recent shock waves studies by Frank and Just[70] indicate that this is the case. These measurements lead to a value of k_3 over the temperature range 1700–2600 K of

$$k_3 \simeq 2.5 \times 10^{-11} \text{ cm}^3 \text{ molecule}^{-1} \text{ s}^{-1}$$

(or $k_3 = 10^{10.18}$ L mol^{-1} s^{-1}). These new data of this very important chain-branching reaction of many combustion systems agree with our predictions within about 10%. This remarkable agreement indicates that the HO_2 potential energy surface is very "normal" and corresponds well to standard looseness parameters α on the entrance and exit sides. Because of the eminent importance of the $H + O_2 \rightarrow HO + O$ chain-branching process in many hydrocarbon oxidation systems, new careful experiments are clearly required in order to check our theoretical suggestion of too low earlier high-temperature data and Frank and Just's new experimental results.

At low temperatures our calculations on the other hand appear to predict too weak a negative temperature coefficient of k_3. Very recent detailed calculations by Clary[77] using an oxygen-quadrupole–OH-dipole interaction potential do reproduce the experimental trends at low temperatures whereas at high temperatures they agree with our results. Apparently the ultrasimple potential model used so far in our statistical adiabatic channel calculations becomes insufficient at low temperatures when the long-range part of the potential plays an important role.

A further comparison can be made with experiments[41] and trajectory calculations[35] of the hot hydrogen atom reaction $H + O_2 \rightarrow HO + O$. The trajectory calculations using the Melius–Blint surface produced total cross sections which were a factor of 3 smaller than the experimental data. Considering the defects of the Melius–Blint surface, two effects counteract. Even if H and O_2 approach at energies much higher than the small entrance barrier, because of the rigidity of the Melius–Blint surface there should be a markedly too small cross section for formation of HO_2 complexes. On the other hand, the fraction of HO_2 complexes dissociating into $O + OH$ rather than into $H + O_2$ should be increased on the Melius–Blint surface. Apparently the reduction of the cross section because of the rigid entrance valley of the potential is the major effect.

Collisional Energy Transfer of Highly Excited HO_2. The analysis of the limiting low-pressure rate coefficients $k_{rec,0}$ in Table III has led to estimates of the average energies $\langle \Delta E \rangle$ transferred in collisions of highly vibrationally excited HO_2 molecules and a variety of bath gases. These data can be compared with the results of recent trajectory calculations of intermolecular energy transfer of excited HO_2.[30-32] Gallucci and Schatz[30] treated energy transfer and collisional dissociation of HO_2 into $H + O_2$ or $HO + O$ in collisions with He. They employed trajectory calculations using the Melius–Blint surface. Rotationally cold or hot HO_2 molecules were considered. Unfortunately, the transfer of translational energy into rotational and vibrational energy were separated only to a limited extent such that a direct comparison with our experimental results cannot be made in a unique way. Representing their results in the form of collisional transition probabilities $P(E_{int},E'_{int}) \simeq (\gamma/2) \exp(-|E_{int} - E'_{int}|/\gamma)$, Gallucci and Schatz derived $\gamma \simeq 0.1kT$ for collisions of "rotationally cold" molecules and $\gamma \simeq 0.15$ eV for collisions of "rotationally hot" molecules (M = He, temperature range 300–1000 K). If we assume that the rotationally cold case resembles thermal conditions most closely, by the use of the relationship[42] $\langle \Delta E \rangle \simeq -\gamma^2/(F_E kT + \gamma)$ these values can be compared with γ values for M = He from Table III of 1.1 kJ mol^{-1} at 298 K and 1.6 kJ mol^{-1} at 1000 K. Similar orders of magnitude for γ were obtained by Miller and Brown,[31,32] who derived $\gamma \simeq 2.8$ kJ mol^{-1} for $T = 800$ K, M = He, and $J < 10$.

It has to be emphasized that detailed energy-transfer calculations separating vibrational and rotational effects should be incorporated into solutions of the two-dimensional (E,J) master equation such as derived in ref 42; i.e., the solution of eq 18 of the one-dimensional master equation can be applied only within certain precautions to the described detailed energy-transfer calculations. Nevertheless, the present agreement of indirectly measured and calculated $\langle \Delta E \rangle$ values is in accord with earlier observations.[43]

Acknowledgment. Financial support of this work by the Deutsche Forschungsgemeinschaft (SFB 93 "Photochemie mit Lasern") is gratefully acknowledged. C.J.C. thanks the Consejo Nacional de Investigaciones Científicas y Técnicas de la República Argentina for a foreign exchange fellowship.

Registry No. H, 12385-13-6; O_2, 7782-44-7; HO_2, 3170-83-0; NH_3, 7664-41-7; Ar, 7440-37-1; CH_4, 74-82-8; N_2, 7727-37-9; OH·, 3352-57-6.

(70) Frank, P.; Just, Th. *Ber. Bunsenges. Phys. Chem.*, in press.
(71) Lewis, R. S.; Watson, R. T. *J. Phys. Chem.* **1980**, *84*, 3495.
(72) Lii, R. R.; Gorse, R. A.; Sauer, M. C.; Gordon, S. *J. Phys. Chem.* **1980**, *84*, 813. Kircher, C. C.; Sander, S. P. *J. Phys. Chem.* **1984**, *88*, 2082.
(73) Kurasawa, H.; Lesclaux, R., presented in part at the 14th Informal Conference on Photochemistry, Newport Beach, CA, 1980.
(74) Heicklen, J. *AIAA J.* **1967**, *5*, 4.
(75) Slack, M. W. *Combust. Flame* **1977**, *28*, 241.
(76) Peeters, J.; Mahnen, G. *Symp. (Int.) Combust., [Proc.], 1972* **1973**, *14*, 133.
(77) Clary, D. C. *Mol. Phys.* **1984**, 81, 3931.